An Advanced Neutron Absorbing Ti-Gd Alloy: Part 1-Corrosion Behavior in Boric Acid

Do Haeng Hur [*], Young-Bum Chun
Nuclear Materials Research Division, Korea Atomic Energy Research Institute, Daejeon 34057
[*]*Corresponding author: dhhur@kaeri.re.kr*

*Keywords : neutron absorbing material, Ti-Gd alloy, corrosion, Gd-rich phase, boric acid

1. Introduction

Advanced neutron absorber materials must have both an improved neutron absorbing capability and structural function for the safe and efficient storage of spent nuclear fuel. B_4C/Al composites, typical neutron absorber materials for spent fuel storage, have a superior neutron absorption capability, but poor mechanical properties [1-2]. On the contrary, borated stainless steels with a high mechanical strength have a low neutron absorbing capability compared to that of Al-B_4C composites [3-4].

Recently, the Korea Atomic Energy Research Institute has launched a research program on the development of new dual-purpose materials with both neutron absorbing and structural function. In its first phase, Ti-Gd alloys were chosen because Ti alloys have been considered as nuclear waste container materials due to their excellent mechanical and anti-corrosion properties in many countries [5-7]. The density of Ti (4.5 g/cm^3) is also significantly lower than that of 304 stainless steel (8.0 g/cm^3). Consequently, it is hypothesized that an advanced neutron absorber material that has both a neutron absorption and a structural function can be developed by a combination of the superior corrosion and mechanical property of Ti and the excellent thermal neutron cross section of Gd. In this study, we fabricated Ti-Gd alloys with different Gd contents and investigated their corrosion behavior under a simulated spent fuel pool water condition using immersion and electrochemical corrosion tests.

2. Materials and Methods

2.1 Material Preparation

Pure Ti and Ti-Gd alloys were fabricated with Ti and Gd lumps (99.95% purity) by plasma arc melting in a chamber filled with argon gas at a pressure of 200 kPa. The ingots were soaked at 1150 °C for 30 min and then hot-forged into 10 mm-thick bars. The bars were hot-rolled at 1000 °C with a thickness reduction of approximately 50%. The plates were finally heat-treated at 1000 °C for 40 min and air-cooled. The chemical compositions of the materials are listed in Table 1.

For microstructure characterization and corrosion tests, one side of each flat specimen was abraded and finished with 2000 grit silicon carbide paper and the other side was further polished with 0.03 μm alumina powder. The specimens were then cleaned in acetone, rinsed in deionized water using an ultrasonic cleaner, and dried with compressed air.

Table 1: Chemical compositions of test materials

Material	Ti	Gd (wt. %)	O (wt. ppm)	N (wt. ppm)
Pure Ti	Balance	0	1040	2
Ti-3Gd	Balance	2.97	900	6
Ti-5Gd	Balance	4.81	980	4
Ti-10Gd	Balance	9.68	1000	N.D.

2.2 Corrosion Tests

Immersion corrosion tests were performed in boric acid(H_3BO_3) solution with 3,000 wt. ppm B at 50 °C. The solution was not deaerated to simulate a pool storage condition. The corrosion coupons were removed from the corrosion cell every 500 h, rinsed in deionized water, and dried with compressed air for weight measurement. The weights of the coupons were measured using a precision electronic balance with a readability of 10 μg. After that, the coupons were returned to the cell filled with new test solution.

Potentiodynamic polarization curves were obtained using polished specimens in boric acid(H_3BO_3) solution with 3,000 wt. ppm B at 50 °C. After the OCP of a working electrode was stabilized, polarization curves were measured from -0.4 V to $+2.5$ V vs. the OCP at a scan rate of 0.5 mV/s.

2.3 Characterization of Microstructure and Corrosion Morphology

The microstructure and chemical compositions of the test materials were analyzed using an optical microscope, and scanning electron spectroscopy (SEM) and energy dispersive spectroscopy (EDS) operating at an acceleration voltage of 15 kV.

After the immersion corrosion tests, the corrosion morphology was observed using SEM. The corroded surface was also cross-sectioned to trace the corrosion paths in the depth direction using the focused ion beam milling technique with a gallium ion beam at a beam energy of 30 keV.

3. Results and Discussion

3.1 Microstructure

As shown in Fig. 1, the microstructure of the Ti-Gd alloys were composed of black particles and the alpha Ti matrix. The size and fraction of the particles increased with the increment of the Gd content. The particles were identified as a Gd-rich phase by EDS analyses. The average chemical composition of several particles was 95.69 Gd, 3.96 Ti, and 0.35 O in wt.%.
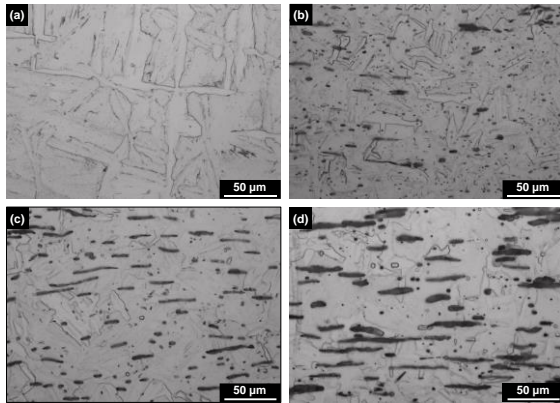
Fig. 1. Optical microstructure (a) pure Ti, (b) Ti-3% Gd, (c) Ti-5% Gd, and (d) Ti-10% Gd.

3.2 Polarization Behavior

Fig. 2 shows the potentiodynamic polarization curves of pure Ti and Ti-Gd alloys in a test solution containing 3,000 wt. ppm B at 50 °C. The corrosion potential (E_{corr}) was shifted to the negative direction and the corrosion rate (I_{corr}) increased by the addition of Gd. Pure Gd exhibited the lowest corrosion potential and the highest corrosion current density among the test materials, resulting in a decrease in the corrosion potential and an increase in the corrosion rate and passive current density of Ti-Gd alloys. The corrosion potential of pure Gd (-0.782 V_{SCE}) was approximately 390 mV lower than that of pure Ti (-0.394 V_{SCE}). This indicates that pure Gd and Ti act as an anode and a cathode, respectively, when they are electrically coupled. Therefore, it is expected that Gd-rich particles dispersed in the Ti matrix dissolve preferentially in the test solution.

3.3 Immersion Corrosion Behavior

Fig. 3 shows the SEM micrographs of the surfaces after the immersion tests for 1500 h. Pure Ti showed no evidence of localized corrosion attack, while Gd-rich particles were dissolved. The corrosion behavior observed in the Ti-Gd alloys is entirely in line with the result predicted from the polarization curves.

Fig. 4 shows the weight loss curves of the test materials with test time in the boric acid solution

containing 3,000 wt. ppm B. The weight loss of pure Ti was negligible, whereas Ti-Gd alloys exhibited relatively large weight loss. Nevertheless, it should be highlighted that the corrosion rates of the alloys are extremely low: the weight loss of Ti-10Gd was 0.35 mg/cm^2 for 1500 h, corresponding to 0.0045 mm/year. This value is much less than those of Al-B$_4$C composites tested under the conditions similar to this work, which are in the range of 0.011~0.043 mm/year [8,9].
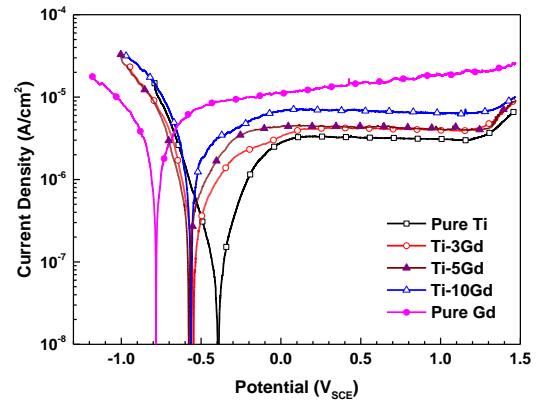
Fig. 2. Potentiodynamic polarization curves of the test materials.
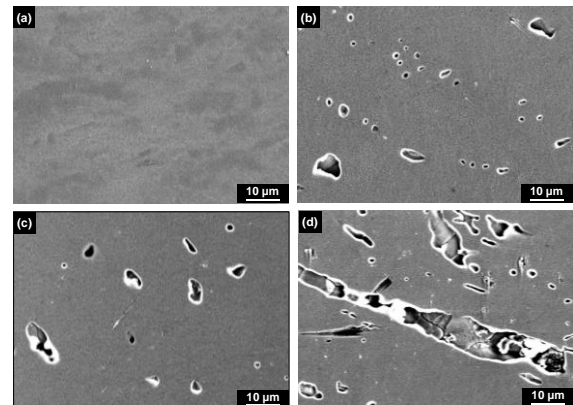
Fig. 3. SEM images after the immersion tests for 1500 h: (a) pure Ti, (b) Ti-3% Gd, (c) Ti-5%-Gd, and (d) Ti-10% Gd.
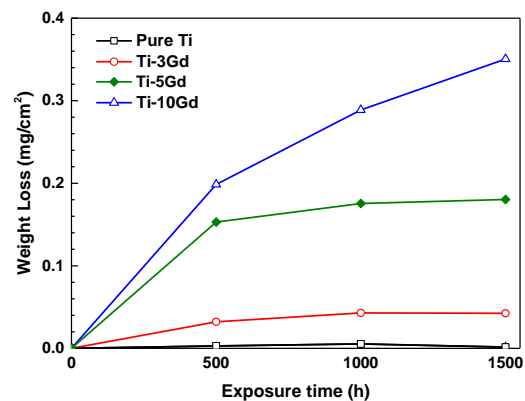
Fig. 4. Immersion corrosion behavior of the test materials in the boric acid at 50 °C.

4. Conclusions

Ti-Gd alloys showed lower corrosion potential, higher corrosion current density, and greater weight loss in the boric acid solution, compared to pure Ti. The reduction in the corrosion resistance of Ti-Gd alloys was attributed to the preferential dissolution of Gd-rich particles in the matrix. However, the corrosion rates of the alloys were much lower than those of Al-B_4C composites. Therefore, Ti-Gd alloys are expected to contribute to spatial integration and weight lighting of dry storage casks as well as fuel pool racks.

5. Acknowledgements

REFERENCES

[1] P. Zhang, Y. Li, W. Wang, Z. Gao, B. Wang B, The design, fabrication and properties of B_4C/Al neutron absorbers, J. Nucl. Mater., Vol.437, p.350, 2013.
[2] H.S. Chen, W.X. Wang, Y.L. Li, et al., The design, microstructure and tensile properties of B_4C particulate reinforced 6061 Al neutron absorber composites, J. Alloys Compd., Vol.632, p.23, 2015.
[3] ASTM−A887−20. Standard Specification for Borated Stainless Steel Plate, Sheet, and Strip for Nuclear Application: ASTM International, USA; 2020.
[4] E.A. Loria, H.S. Isaacs, Type 304 stainless steel with 0.5% boron for storage of spent nuclear fuel, JOM, Vol.32, p.10, 1980.
[5] F. King, Container materials for the storage and disposal of nuclear waste, Corrosion, Vol.69, p.986, 2013.
[6] F. Hua, K. Mon, P. Pasupathi, G. Gordon, D. Shoesmith, A review of corrosion of titanium grade 7 and other titanium alloys in nuclear waste repository environments, Corrosion, Vol.61, p.987, 2005.
[7] Q. Zhang, M. Zheng, Y. Huang, et al., Long term corrosion estimation of carbon steel, titanium and its alloy in backfill material of compacted bentonite for nuclear waste repository, Scientific Reports, Vol.9, p.3195, 2019.
[8] Y.-L. Li et al., Corrosion behavior of B_4C/6061Al neutron absorber composite in different H_3BO_3 concentration solutions, Acta Metall. Sin., Vol.29, p.1037, 2016.
[9] R.E. Fuentes et al., Electrochemical testing of aluminum-boron carbide cermet panels from the decommissioned Zion nuclear power plant spent fuel pool, CORROSION 2021, Paper No. 16548, NACE, USA, 2021.